JOURNAL OF MATERIALS SCIENCE **39** (2004) 5379– 5383

Application of AFM to study functional nanomaterials prepared by mechanical alloying

J. JAKUBOWICZ*
Institute of Materials Science and Engineering, Poznan University of Technology, M. Sklodowska-Curie 5 Sq., 60-965 Poznan, Poland
E-mail: jjakubow@sol.put.poznan.pl

Two-phase hard magnetic $Nd_2Fe_{14}B/\alpha$-Fe nanocomposites and nanocrystalline TiFe electrode materials were prepared by mechanical alloying and heat treatment. The microstructure of both types of functional nanomaterials was investigated by atomic force microscopy. In the case of $Nd_2Fe_{14}B$ magnetic phase, the microstructure refinement was realised by careful heat treatment and Zr addition. AFM investigations showed that Zr reduces a grain size of a parent alloy in the range of 20–40%. More than 90% grains have size below 50 nm, and more than 50% grains have size below 20 nm, which results in enhanced remanence. On the other hand, in TiFe alloy, a fine microstructure is known to improve greatly the properties of hydrogen storage alloys, when compared with their conventional polycrystalline counterparts. Additionally, the substitution of Fe by some amount of nickel improves the activation property of TiFe. Two types of AFM imaging modes, height and deflection, are accurate for agglomerate and grain size presentation, respectively.

1. Introduction

The most promising method for the preparation of various nanocrystalline compounds is mechanical alloying (MA) of elemental powders [1]. In this simple technology, the powders are crushed and welded together between the steel balls and the walls of the mill. The process leads to the formation of amorphous materials as well as to a fine grain structure.

In nanocomposite magnets based on hard-soft magnetic $Nd_2Fe_{14}B/\alpha$-Fe phases, the nanometer size grains result in the presence of an exchange coupling between them [2], resulting in a spin reorientation in the coupled area of the soft grains. This implies a higher remanence than in isotropic microcrystalline counterparts. When the grains are smaller, the higher is the volume of the grain that becomes affected under the influence of exchange bonds. In order to achieve optimum magnetic properties in isotropic nanocrystalline $Nd_2Fe_{14}B/\alpha$-Fe magnets, a mean grain size of 20 nm is required [2]. Technologically useful values of coercivity, ${}_JH_c$, in nanocomposites are maintained for volume fractions of the soft phase up to 40% [3]. To suppress growth of the grains, resulting in high coercivity, refractory elements such as Zr, V, Nb, Mo, W, V should be added [4].

The mechanical alloying can be applied for preparation of metal hydride materials with high storage capacity. Among the different types of hydrogen forming compounds, Ti-based alloys are promising materials for hydrogen energy applications [5]. The TiFe alloy is lighter and cheaper than the $LaNi_5$-type alloys and can absorb up to 2 H/f.u. at room temperature. The replacement of Fe by some amount of another transition metal results in the improvement of the poor activation property of TiFe [6, 7]. The ball milling of TiFe is effective for the improvement of the initial hydrogen absorption rate, due to the reduction in the particle size and to the creation of new clean surfaces [8, 9].

Atomic force microscopy has been applied with success in imaging many types of materials. This technique offers the highest resolution and the simplest preparation from all types of scanning probe microscopes (SPM) and electron microscopes (SEM, TEM). Some authors report the AFM investigations of ribbons of melt spun nanomaterials [10], but application of AFM to the study of nanopowders has been reported in only few papers. In the present study, AFM has been applied for the microstructure imaging of mechanically alloyed $Nd_2Fe_{14-x}Zr_xB/\alpha$-Fe ($x = 0, 0.5$) and $TiFe_{1-x}Ni_x$ ($x = 0$, 0.25, 0.5, 0.75 and 1.0) powders.

2. Experimental details

Magnets with composition $Nd_2Fe_{14}B$/37.5 vol% α-Fe and $Nd_2Fe_{13.5}Zr_{0.5}B$/37.5 vol% α-Fe were prepared from high purity elemental Nd, Fe, Zr, B powders, using a SPEX 8000 mill. Hardened steel containers including steel balls and powders have been applied in the mechanical alloying process. Powder handling was done in a glove box with automatically controlled atmosphere. Mechanical alloying has been done in an argon atmosphere. The mill was run for 48 h and the original

*Author to whom all correspondence should be addressed.

powder mixture was transformed into an amorphous (Nd, B)—crystalline (α-Fe) material. The amorphous $Nd_2Fe_{14}B/\alpha$-Fe structure crystallizes after heat treatment under argon atmosphere in the temperature range of 600–800°C.

Mechanical alloying of TiFe alloys was carried out in the same setup as in the case of magnetic materials. The $TiFe_{1-x}Ni_x$ with $x = 0$, 0.25, 0.5 and 0.75 were prepared. The mill with elemental powders of Ti, Fe and Ni was run up to 44 h for each powder preparation. The as-milled powders were heat-treated at 700°C for 0.5 h under high purity argon. The mechanically alloyed and annealed materials were electrochemically measured as working electrodes. The procedure of electrochemical measurements is described elsewhere [11].

The microstructure was determined by AFM (Nanoscope IIIa, Digital Instruments, USA). The AFM contact mode operation with a supersharp n^+Si tip was applied. Due to lateral forces in the contact mode operation (tip dragged on the surface) and to prevent any artefacts, the powders were fixed to the ground. A scan rate below 2 Hz was applied to avoid powder movements. In the contact mode operation, two types of images have been taken at a time. The structure features were reflected by changes in height and deflection bending of the cantilever.

3. Results and discussion

3.1. $Nd_2Fe_{14}B/\alpha$-Fe nanocomposite magnets

After 48 h of mechanical alloying, the elemental powder mixture transforms into highly dispersed α-Fe crystallites located in an amorphous Nd-B or Nd-Zr-B matrix. Heat treatment of the mechanically alloyed powders results in crystallization of the $Nd_2Fe_{14}B$ phase, which is exchange coupled with the α-Fe phase.

Fig. 1 shows AFM deflection images and grain size distributions of $Nd_2Fe_{14}B$/37.5 vol% α-Fe after 48 h of mechanical alloying (a), and after mechanical alloying and heat treatment (at 700°C for 30 min) (b). After MA, the average grain size (mixture of α-Fe crystallites and particles of the amorphous phase) is equal to 38 nm. After heat treatment at 700°C for 30 min, the nanocrystalline $Nd_2Fe_{14}B$ (with the average grain size of about 26 nm) crystallizes from the amorphous phase.

The addition of refractory Zr suppresses grain growth as well as ensures a refined homogeneous structure (Fig. 2). AFM deflection images and grain size distributions clearly indicate refinement of the structure in comparison to a nanocomposite without Zr (Fig. 1). After mechanical alloying, the average grain size of the mixture of Zr-added $Nd_2Fe_{13.5}Zr_{0.5}B$/37.5 vol% α-Fe is equal to 28 nm ((Fig. 2a), and after heat

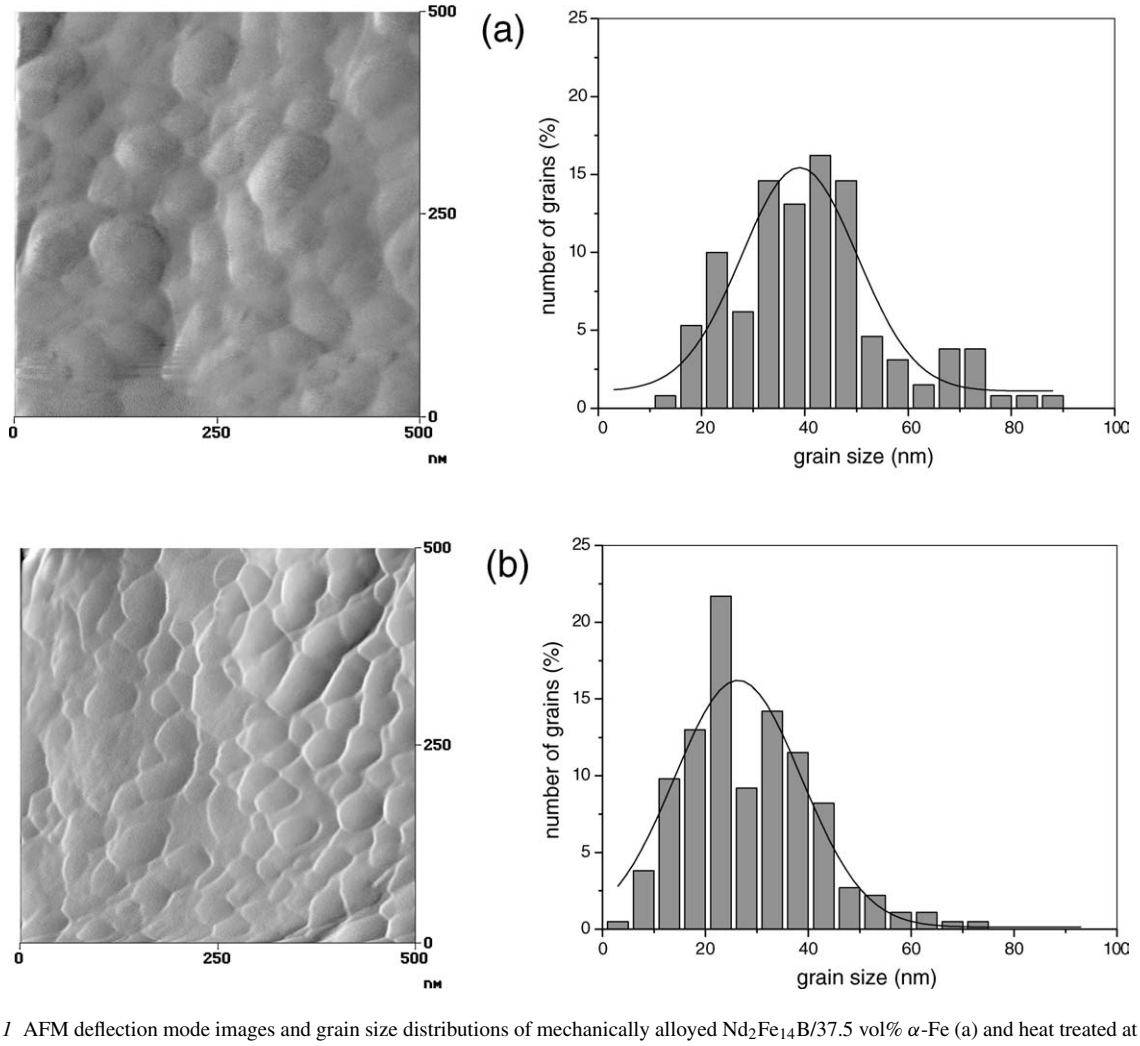

Figure 1 AFM deflection mode images and grain size distributions of mechanically alloyed $Nd_2Fe_{14}B$/37.5 vol% α-Fe (a) and heat treated at 700°C for 30 min (b).

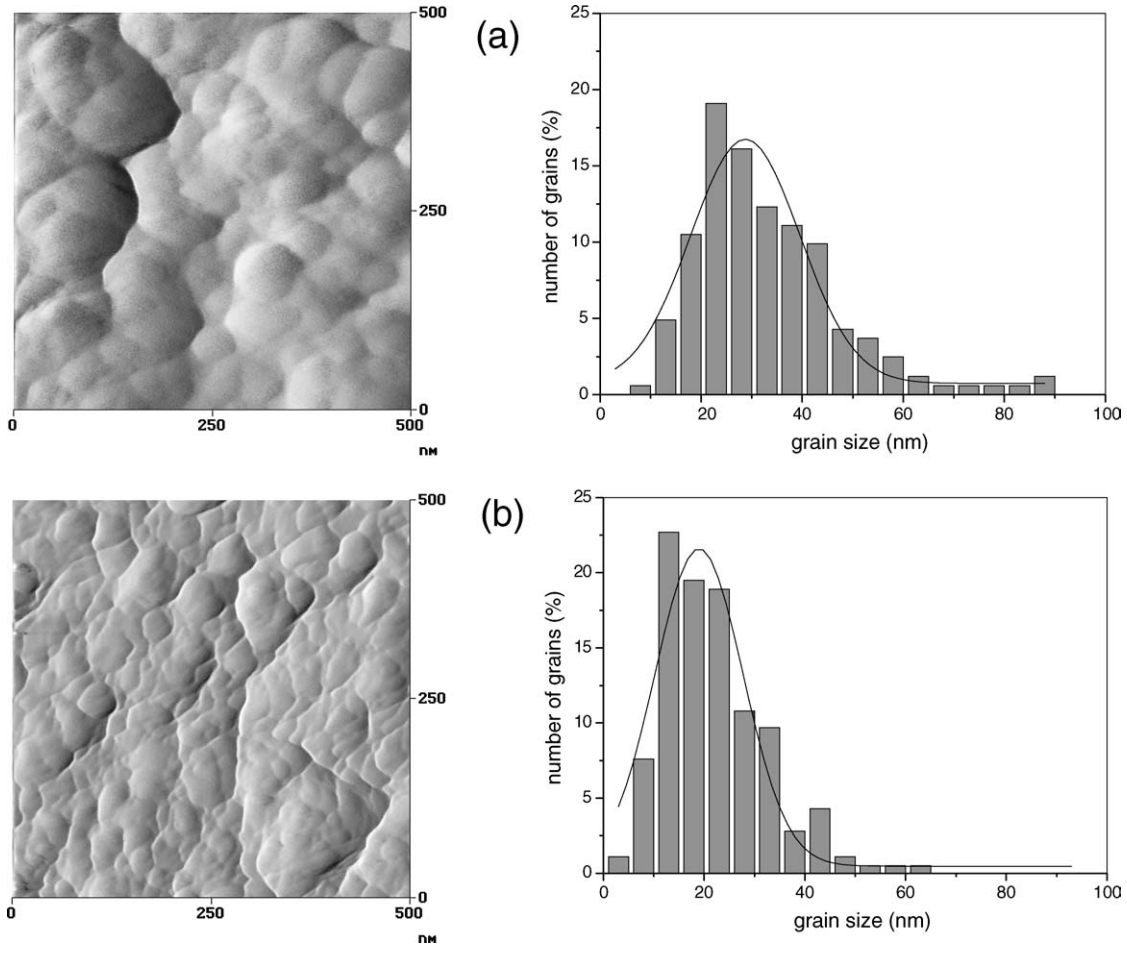

Figure 2 AFM deflection mode images and grain size distributions of mechanically alloyed $Nd_2Fe_{13.5}Zr_{0.5}B$/37.5 vol% α-Fe (a) and heat treated at 700°C for 30 min (b).

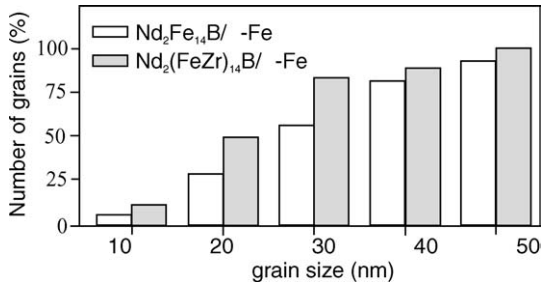

Figure 3 Number of grains with different sizes after heat treatment at 700°C for $Nd_2Fe_{14}B$/37.5 vol% α-Fe and $Nd_2Fe_{13.5}Zr_{0.5}B$/37.5 vol% α-Fe.

treatment at (at 700°C for 30 min) it is estimated to be about 19 nm. Thus, Zr reduces the grain size distribution [12]. Fig. 3 shows how many grains lie below the established level of the grain size after MA and heat treatment at 700°C for $Nd_2Fe_{14}B$/37.5 vol% α-Fe and $Nd_2Fe_{13.5}Zr_{0.5}B$/37.5 vol% α-Fe. In both cases, at 700°C, more than 90% of the grains have a size below 50 nm. The $Nd_2Fe_{13.5}Zr_{0.5}B$/37.5 vol% α-Fe nanocomposite has more grains with smaller size in comparison to $Nd_2Fe_{14}B$/37.5 vol% α-Fe. The number of grains below (or equal) 20 nm is 50 and 27% for $Nd_2Fe_{13.5}Zr_{0.5}B$/37.5 vol% α-Fe and $Nd_{12.6}Fe_{81.4}B_6$/37.5 vol% α-Fe, respectively. The difference in the grain size with and without Zr-containing nanocomposite increases with increasing heat treatment temperature [12]. For melt-spun nanocomposites, the average grain size of α-Fe is 10–15 nm and of $Nd_2Fe_{14}B$ is 15–40 nm [13, 14]. These data are comparable with the results obtained here.

In comparison to the results of high-energy ball-milling presented in [15], agglomerates and/or aggregates composed of smaller grains are formed after mechanical alloying. The size of the agglomerates lies, in general, below 250 nm (Fig. 4). The agglomerates are clearly visible in AFM height mode images (Fig. 4a). Smaller crystallites are better visible in AFM deflection mode images (Fig. 4b).

3.2. TiFe electrodes

The powder mixture milled for 44 h has transformed completely to the amorphous phase, without formation of another phase [11]. Formation of the nanocrystalline TiFe alloy was achieved by annealing the amorphous material under a high purity argon atmosphere at 700°C for 0.5 h. The TiFe has CsCl-type structure with cell parameter $a = 2.973$ Å. When nickel is added to $TiFe_{1-x}Ni_x$, the lattice constant a increases (Table I). The crystallite size of the nanocrystalline TiFe powders was below 50 nm; a lot of grains with the size of about 30 nm is clearly visible (Fig. 5).

Table I includes also the discharge capacities of the materials. The discharge capacity of the parent TiFe electrodes is very low. The substitution of Fe by Ni in

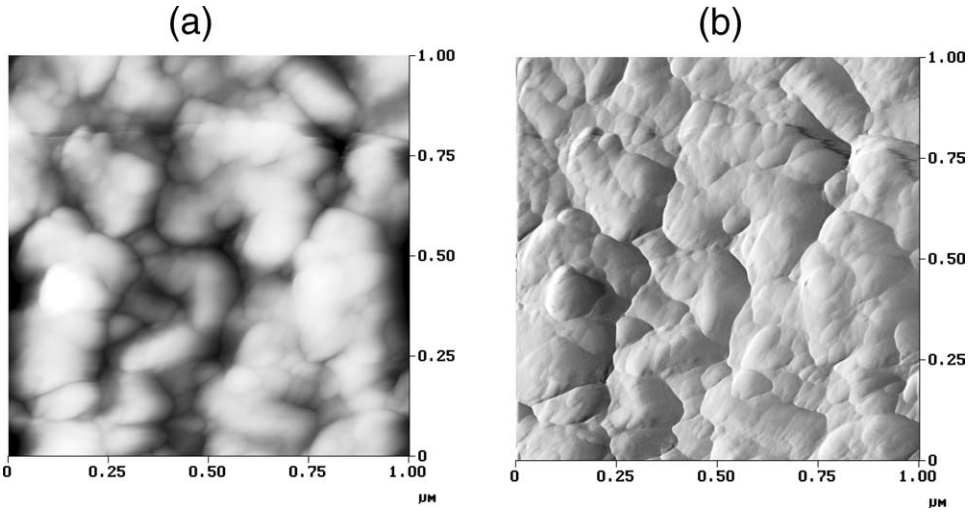

Figure 4 AFM height mode (a) and deflection mode (b) images of agglomerates of the $Nd_2Fe_{14}B$/37.5 vol% α-Fe mechanically alloyed and heat treated at 700°C for 30 min.

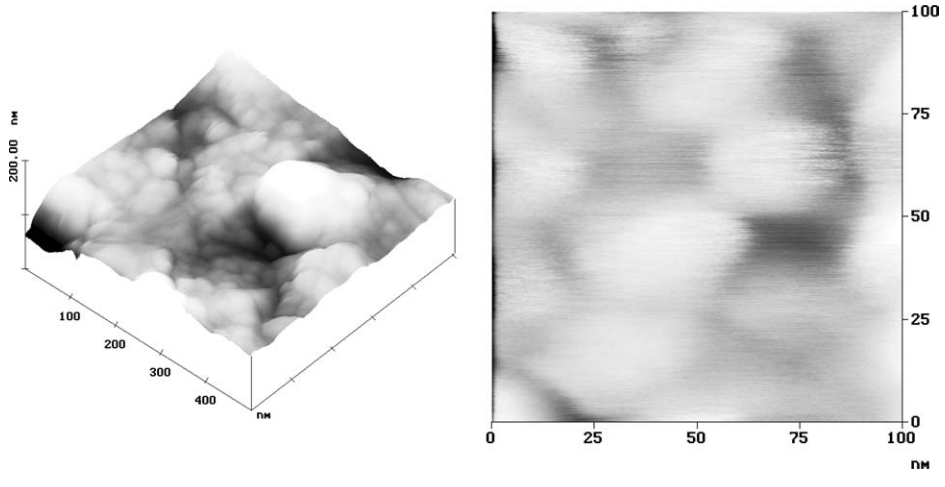

Figure 5 AFM height mode images of the mechanically alloyed and heat treated (at 700°C for 30 min) TiFe powders.

$TiFe_{1-x}Ni_x$ leads to an improvement in activation behavior of the electrodes. It was found that the increasing nickel content in $TiFe_{1-x}Ni_x$ alloys leads initially to an increase in discharge capacity, giving a maximum at $x = 0.75$. The annealed nanocrystalline $TiFe_{0.25}Ni_{0.75}$ powder has discharge capacity of 155 mA h g^{-1}. The electrodes displayed maximum capacities at around the third cycle [11]. It is important to note that the mechanically alloyed TiFe alloys exhibited higher discharge capacities than the arc melted ones [16]. The size reduction of the powder particles and the creation of a new surfaces are effective for the improvement of the hydrogen absorption rate.

TABLE I Structural parameters and discharge capacities for nanocrystalline $TiFe_{1-x}Ni_x$ materials (current density of charging and discharging was 40 mA g^{-1})

Composition	a (Å)	V (Å)	Discharge capacity on third cycle (mA h g^{-1})
TiFe	2.973	26.28	0.7
$TiFe_{0.75}Ni_{0.25}$	2.991	26.76	55
$TiFe_{0.50}Ni_{0.50}$	3.001	27.03	125
$TiFe_{0.25}Ni_{0.75}$	3.010	27.27	155
TiNi	3.018	27.49	67

4. Conclusion

The $Nd_2Fe_{14}B$/37.5 vol% α-Fe and $Nd_2Fe_{13.5}Zr_{0.5}$-B/37.5 vol% α-Fe nanocomposite magnets have been prepared by mechanical alloying. Zr additive reduces the grain size, grain size distribution and suppresses grain growth during heat treatment. The $Nd_2Fe_{14}B$/37.5 vol% α-Fe and $Nd_2Fe_{13.5}Zr_{0.5}B$/37.5 vol% α-Fe nanocomposites were produced with the grain size of 27 nm and 19 nm, respectively. Zr reduces the grain size of the parent structure from 20 to 40%. Nanocrystalline $TiFe_{1-x}Ni_x$ alloys are used as the negative electrode materials for a Ni-MH_x battery. It was found that the increasing nickel content in $TiFe_{1-x}Ni_x$ alloys leads initially to an increase in discharge capacity, giving a maximum at $x = 0.75$. In the nanocrystalline $TiFe_{0.25}Ni_{0.75}$ powder with the average crystallite size of 30 nm, discharge capacities of up to 155 mA h g^{-1} were measured.

Acknowledgement

The AFM investigations were done at the Hahn-Meitner-Institut Berlin GmbH. The financial support of the Polish National Committee for Scientific Research (KBN) under the contract No KBN 8T10A 001 20 is gratefully acknowledged.

References

1. W. GONG, G. C. HADJIPANAYIS and R. F. KRAUSE, *J. Appl. Phys.* **75** (1994) 6649.
2. E. F. KNELLER and R. HAWIG, *IEEE Trans. Magn.* **27** (1991) 3588.
3. M. JURCZYK and J. JAKUBOWICZ, *J. Magn. Magn. Mater.* **185** (1998) 66.
4. M. JURCZYK, *J. Alloys Comp.* **235** (1996) 232.
5. L. ZALUSKI, A. ZALUSKA and J. O. STRÖM-OLSEN, *ibid.* **253/254** (1997) 70.
6. B. LUAN, N. CUI, H. K. LIU, H. J. ZHAO and S. X. DOU, *J. Power Sources* **55** (1985) 197.
7. S. M. LEE and T. P. PERNG, *J. Alloys Comp.* **291** (1999) 254.
8. H. AOYAGI, K. AOKI and T. MASUMOTO, *ibid.* **231** (1995) 804.
9. C. B. JUNG, J. H. KIM and K. S. LEE, *Nanostruct. Mater.* **8** (1997) 1093.
10. M. A. AL-KHAFAJI, W. M. RAINFORTH, M. R. J. GIBBS, H. A. DAVIES and J. E. L. BISHOP, *J. Magn. Magn. Mater.* **188** (1998) 109.
11. M. JURCZYK, E. JANKOWSKA, M. NOWAK and J. JAKUBOWICZ, *J. Alloys Compd.* **336** (2002) 265.
12. J. JAKUBOWICZ, *ibid.* **351** (2003) 196.
13. B. Z. CUI, X. K. SUN, W. LIU, D. Y. GENG, Z. Q. YANG and Z. D. ZHANG, *ibid.* **302** (2000) 281.
14. Y. Q. WA, D. H. PING, K. HONO, M. HAMANO and A. INOUE, *J. Appl. Phys.* **87** (2000) 8658.
15. M. JURCZYK and J. JAKUBOWICZ, *J. Alloys Compd.* **311** (2000) 292.
16. C. B. JUNG and K. S. LEE, *ibid.* **253/254** (1997) 605.

Received 11 September 2003
and accepted 27 February 2004